Anti-icing and de-icing coatings based Joule's heating of graphene nanoplatelets

O. Redondo[a,*], S.G. Prolongo[a], M. Campo[a], C. Sbarufatti[b], M. Giglio[b]

[a] Universidad Rey Juan Carlos, ESCET, Área de Ciencia e Ingeniería de Materiales, C/Tulipán s/n, Móstoles, 28933, Madrid, Spain
[b] Politecnico di Milano, Dipartimento di Meccanica, Via La Masa 1, 20156, Milano, Italy

Epoxy coatings doped with graphene nanoplatelets (GNP) with average thickness close to 200 μm have been manufactured on glass fibre laminate substrate. Their electrical conductivity was close to 0.001–0.01 S/m be-cause the GNP percentages added (8–12 wt% GNP) were higher than the electrical percolation threshold of this GNP/epoxy system. The electrical current increases exponentially with the applied voltage due to the self-heating of the samples. Therefore, these materials don't follow the Ohm's law. Interestingly, the electrical re-sistance remains constant, or even decreases, at cryogenic temperatures. Self-heating of GNP/epoxy coatings due to Joule's effect was also studied, analysing the effect of the applied voltage. The coating doped with the highest GNP content presented more efficient heating due to its higher electrical conductivity and therefore higher transported electrical current.

The application of a relatively high voltage, 750–800 V, induced the self-heating of materials, which was used for anti-icing and de-icing applications. Different thermoelectrical tests at low temperatures, between −10 and

− 30 °C, have been designed and carried out, confirming the high efficiency of these materials as an anti-icing and de-icing system (ADIS) which required low electrical power, close to 2.5 W, showing a short time to melt the ice and high reproducibility.

1. Introduction

Ice formation reduces the efficiency of numerous outdoor devices in severe weather conditions. Among these devices are wind turbines and aircrafts. Different anti-icing systems, with the function of preventing the ice formation, and de-icing devices, with the capacity to melt or separate the ice from the substrate material, jointly named ADIS (anti-icing and de-icing system), are being developed [1,2].

Most of the anti-icing approaches available in the literature are passive, and rely on a hydrophobic substrate material which limits ice formation on the system's surface [3,4], whereas de-icing is usually performed by means of active approaches. One typical de-icing device is based on the melting of ice via hot air or other fluids propelled by a high-pressure compressor. The efficiency of these de-icing systems is high, but their response time is too long [2]. More complex active systems based on smart memory alloys exploit the high deformation of a substrate layer in contact with the ice, consequently separating the ice from the substrate material under the system vibrations. However, the structural complexity of this de-icing approach has limited its application in real environments. There are rare demonstrations available in the literature of systems possessing both anti-icing and de-icing properties. Very recently, a thermomechanical ADIS based on a bi-stable laminate composite structure with a superhydrophobic surface has been presented in Ref. [5].

In this work, the authors proposed the application of epoxy coatings doped with graphene nanoplatelets (GNP) as an ADIS, using the self-heating caused by Joule's effect; few studies have been found in the bibliography about the development of these self-heating materials [1,2]. Epoxy resins are extensively used as protective coatings of composite materials due to their excellent adhesive properties and high heat resistance. On the other hand, graphitic nanoparticles have been widely studied as nanofillers during the last decade, to enhance the mechanical, thermal, electrical, and barrier properties of polymers [6,7]. Recent studies have confirmed that the reinforcement of epoxy coatings with GNP allows coatings with improved wear strength to be obtained [6]. Moreover, if the GNP concentration is higher than the electrical percolation threshold, the doped coating becomes a conductor, enhancing the electrical discharge in wet environments. However, the values of electrical conductivity reached for GNP/epoxy composites are relatively low, close to 10^{-3} S/m [7].

Received 7 February 2018;
Received in revised form 8 May 2018;
Accepted 18 May 2018
Available online 19 May 2018

* Corresponding author.
E-mail address: osiris.redondo.herrero@urjc.es (O. Redondo).

When a voltage difference is applied to the conductor material, the electric current flows through the conductor. The electrical energy is expended in overcoming the frictional resistance between the electrons and the atoms or molecules of the material. According to the law of energy conservation, this electrical energy must be converted into some other form of energy – heat – thus increasing the temperature of the conductor material. This heating is known as Joule's effect. The amount of heat produced is proportional to the square of the current, the resistance of the circuit, and the duration for which the current flows through the circuit. Recent published works [8,9] used this heating for de-icing applications, showing promising results. The investigated materials were resins doped with carbon nanotubes (CNTs) as electrical nanofillers. It is well known that the percolation threshold of these nanocomposites is usually lower than those doped with GNP and, in addition, their electrical conductivity is usually higher [10].

The main goal of this study is the development of a new ADIS based on an epoxy coating doped with GNPs. Graphene presents several advantages as a nanofiller for this application; among them, high thermal conductivity (around 500–5000 W/mK) [11] and excellent barrier properties. ADIS coatings require both electrical conductivity and high thermal conductivity to ensure homogeneous heating. Different tests have been designed and carried out in order to determine the behaviour of GNP/epoxy composites at different low temperatures, above and below 0 °C. The effect of different experimental conditions, such as the applied voltage, the electrical conductivity of the coating, and the environmental temperature, have been analysed to determine the ability and efficiency of these materials for both de-icing and anti-icing applications. In addition, the reproducibility of this new ADIS has been confirmed by repeated testing.

2. Experimental activity

2.1. Materials

Nano-reinforced epoxy coatings were manufactured using GNPs as nanofillers, purchased from XGScience (commercial grade M25), with an average thickness of 6–9 nm and 25 μm lateral size. The epoxy matrix was a commercial two-component epoxy resin, specially designed for coatings with room temperature curing and low density. This resin is commercially named EPOLAM, provided by Axon Technologies. A glass fibre–epoxy laminate, supplied by Rochling Composites, was used as a substrate.

2.2. Sample preparation

Different GNP percentages (8, 10, and 12 wt%) were added to manufacture the nano-reinforced coatings, together with pristine epoxy resin as reference. GNPs were dispersed into the epoxy monomer by a three-roll mill (Exakt 80 E, supplied by Exakt GmbH). The mechanical dispersion was optimised previously [12–14], with a controlled gap and roller speed, and the application of suitable shear forces to disperse and stretch the nanoplatelets. The epoxy monomer was then degassed at 40 °C for 2 h, after which the amine hardener was added, and mixed by a calendering process. The final mixture was applied onto the laminate substrate using a special rectangular metal film applicator with a 200 μm gap. The substrate was previously treated by shot-peening with sand, to increase its roughness and to enhance the coating–substrate adherence. Finally, the epoxy coating was cured at 23 °C for 24 h and then postcured at 40 °C for 10 h.

For anti-icing and de-icing tests, substrates of 100 × 20 mm were coated with GNP/epoxy coatings, with an average thickness of 194 ± 22 μm. Then, two single copper wires of 200 μm diameter were located on two thin silver lines that were painted on the coating, separated by 20 mm. The wires were fixed by a hot melting adhesive and then painted again with silver to ensure good electrical contact with the coating. The electrical contacts were electrically insulated with a special resin to avoid short circuits due to contact with water or moisture. Fig. 1 represents a scheme of the geometry and the electrical distribution of the samples tested.

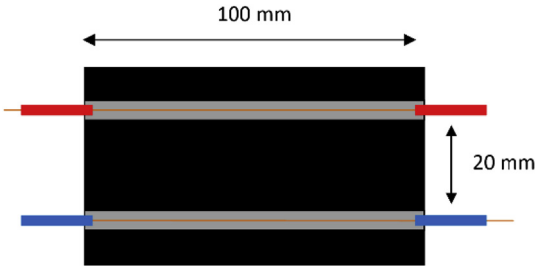

Fig. 1. Scheme of the geometry and electrical configuration of the samples for electrical and thermoelectrical tests.

2.3. Characterisation and experimental tests

The morphology of the nano-reinforced coatings was studied by scanning electron microscopy (SEM-EDX, Hitachi S-2400 N). The sample's surface was first coated with a thin Au (Pd) layer of 5–10 nm by sputtering. The sputtering conditions were 30 mA and 120 s (Bal-tec, SCD-005 sputter).

The adhesion strength of the coatings to the composite substrates was measured by the pull-off adhesion test, using a Posi Test AT-Pull-Off Adhesion Tester, following the ASTM D4541-02 standard, procedure E.

Current–voltage (I–V) electrical measurements were carried out with different electrical source and meter devices. An electrical source (PSM 2/2 A 2CH) with an electrical amplifier (BURLEIG High Voltage DC Op Amp PZ-70) allowed the application of different electrical voltages, from 0.1 to 1000 V. The electrical measurements were done with a multimeter (FLUKE 45) to measure the voltage, and a multimeter (AGILENT) to measure the electrical current. All electrical measurements were made in direct current (DC). Fig. 2 shows a picture and a scheme of the equipment used.

Two different methods were used to measure the temperature of the samples. The first consisted of a thermal sensor (ATERSID FT 905), which was attached to the coating's surface; the second was a thermal camera (AFlir B335), used to capture thermographs with a 0.95–0.97 emissivity. A thermal camera recorded images of the radiations emitted by the sample. The measured radiation of the camera does not depend only on the sample temperature; it is affected by radiation from the environment and by the emissivity of the sample. Therefore measurements rely on the comparison between the radiation emitted by the coating and a black body at the same standard reference temperature [15]. The thermal camera was placed 40 cm from the samples. Both of these methods allowed measurement of the temperature increase due to Joule's heating.

Three different kinds of thermoelectrical tests were designed for this work. The first one consisted of the analysis of Joule's heating at room temperature, for a preliminary characterisation of the coating performance in absence of ice. While applying different constant electrical voltages, the electrical current was measured, together with the generated increase of temperature.

The second study consisted of de-icing tests, analysing the ability of the manufactured coatings to melt or remove the adhered ice through the application of a constant electrical voltage. Finally, anti-icing tests were also designed and executed, verifying the coating's ability to avoid ice formation by applying a constant electrical voltage while the sample was subject to a severe wet and cold atmosphere.

For the first thermoelectrical test, carried out at room temperature, three samples were tested with applied voltages between 0 and 800 V by DC. Each voltage was stabilised for one minute. Then, the amount of

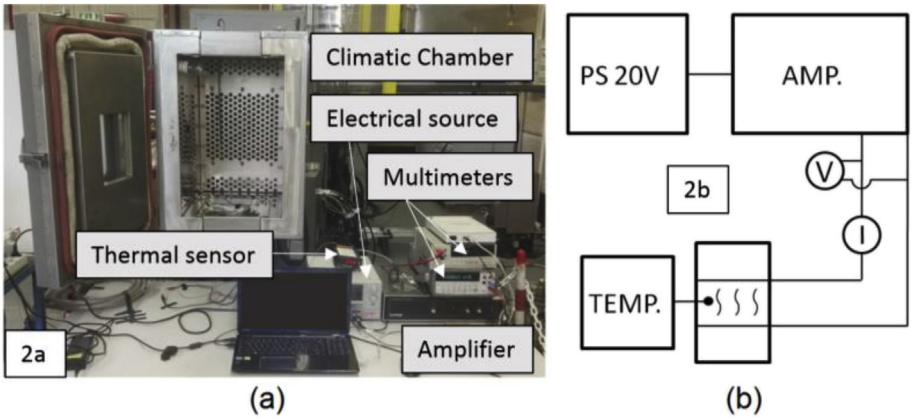

Fig. 2. (a) View of the experimental setup and (b) scheme of the equipment connections.

electrical current transported and the maximum temperature increase of the sample's surface was registered at each applied voltage.

De-icing tests were carried out in a climatic chamber (MTS 651) after creating the ice on some selected regions across the samples at −15 °C. A hollow rectangular mould was placed over the sample, into which 4 ml of distilled water was added. In this way, a homogenous and controlled ice layer was generated across the sample. After the ice was completely formed, the de-icing test consisted of the application of 750 V, using the electrical contacts described in section 2.2. In a first de-icing test, the samples were hung in a vertical position at room temperature and the ice melting process was monitored by temperature measurements using a thermal camera.

Additional de-icing tests were executed in the climatic chamber at different low temperatures, specifically −10, −20, and −30 °C. The procedure for ice generation was the same as before. The difference between the de-icing test at room temperature and at low temperatures was that the tests at low temperature were carried out in the climatic chamber, and therefore the sample's surface temperature had to be measured by a thermal sensor, instead of the thermal camera, for monitoring of the ice's melting and separation process, specifically at the ice–coating interface. Again, a constant voltage, in the range of 750–800 V in DC, was applied between the electrodes located over the surface at 20 mm as can be appreciate in Fig. 1.

Anti-icing tests were aimed at verifying the coating's ability to avoid (or at least to limit) the generation of ice. These tests were carried out in the climatic chamber (MTS 651) at −15 °C. A humidifier (Fog 60), with three sprinklers oriented towards the sample at 37 cm from the sample's surface, was used to ensure a high humidity in the cold atmosphere. Water was repetitively vaporised over the sample surface for 5 s, every 45 s. The anti-icing test consisted of the repetition of this procedure 14 times, while applying 750–800 V at the electrodes and monitoring the temperature of the sample's surface with a thermal sensor (ATERSID FT 905). At the end of each test procedure, the thickness of the ice generated on the non-active surface was measured with a micrometer at some selected locations.

3. Results and discussion

3.1. Characterisation of nano-reinforced coatings

Different GNP/epoxy composite coatings were manufactured, where the GNP percentage was modified from 8 to 12 wt% with respect to the epoxy matrix. The GNP content was relatively high to ensure good electrical conductivity of the samples. Previous published works [16] confirmed that the electrical percolation threshold for these non-functionalised GNPs is close to 5 wt%.

Fig. 3 shows some SEM micrographs of a GNP/epoxy coating over the laminate substrate. Fig. 3a corresponds to the sample cross-section, where a homogenous coating is observed. All studied coatings presented a constant thickness (marked with a white arrow in Fig. 3a), with an average value of 194 ± 22 µm. No differences were observed as a function of the added GNP percentage. The morphological characterisation confirmed that the manufactured coatings are well consolidated and homogenous, without porosity, holes, or cracks at the coating–substrate interface, which implies a good interaction and adherence with the substrate (black rectangle on Fig. 3a). The adherence of the coatings to the composite substrate was measured by the pull-off test. The average value measured for adhesive strength is 5.7 ± 0.2 MPa. The strength of the pristine epoxy coating is similar to that of the nano-reinforced ones. The adhesive strength measured is relative high, as was expected of the epoxy formulation, with low viscosity designed for coatings.

Observing the GNP orientation in the cross-sectional micrograph (Fig. 3a), it was confirmed that there is a slight preferential orientation of nanoplatelets. They are preferentially oriented in a direction parallel to the substrate surface. This self-orientation has been studied in a previous work [17]. Finally, the stratification effect was observed, showing the same GNP concentration throughout the entire thickness of the coating.

SEM micrographs also allow analysis of the distribution of nanoplatelets into the epoxy matrix. For any studied GNP content, it was observed that nanoplatelets are well dispersed in the epoxy matrix, without high aggregates or agglomerations, confirming that the dispersion procedure applied by calendering was suitable. In addition, the nanoplatelets appear to be stretched, without a rolling or wrinkling effect, which enhances the electrical percolation. In fact, one of the main advantages of mini-calendering, in comparison with other conventional dispersion techniques, is the stretching of nanofillers in two nano-dimensions.

Another interesting morphological feature of the studied nano-doped coatings is the partial exfoliation and intercalation effect of the GNPs. Around twenty staked graphitic layers form the neat nanoplatelets. However, the thickness of the GNPs dispersed in the epoxy matrix varies (Fig. 3a and b), corresponding to different numbers of graphitic layers. In fact, it is possible to observe both the intercalation effect (marked with red arrows), where the distance between the graphitic layers are greater than in neat GNPs, and the exfoliation effect (marked with yellow arrows), manifesting through graphitic nanosheets.

The only negative observation of these materials is the different lateral size of the nanoplatelets; the observed GNP length varies from 15 to 100 µm. Considering that the commercial supplier indicates an average lateral size of 25 µm, the length differences must proceed from pristine GNPs and the dispersion procedure applied don't modify it. There does not seem to occur a negative shorting effect caused by the dispersion technique.

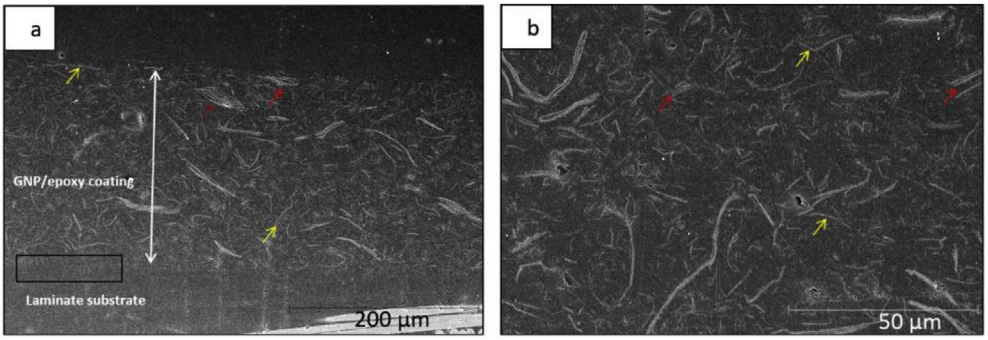

Fig. 3. SEM images of epoxy coating doped with 10 wt% GNP over a laminate substrate, where (a) shows a lateral cross-section and (b) shows the surface morphology. Different morphological features are marked: thickness of coating (white arrow); part of the coating–substrate interface (black rectangle); intercalated nanoplatelets (red arrows); and exfoliated graphitic nanosheets (yellow arrows). (For interpretation of the references to colour in this figure legend, the reader is referred to the Web version of this article.)

3.2. Thermoelectrical characterisation at room temperature

The application of nano-reinforced coatings as an ADIS implies the need of a deep knowledge of their thermoelectrical properties, specifically to determine their ability to conduct the electrical current, and to establish the heating caused by Joule's effect. This study was made hereafter at room temperature.

Joule's heating, also referred to as resistive or ohmic heating, describes the process of heat generation. When an electric current flows through a solid with finite conductivity, electrical energy converts to heat, due to the transfer energy from conducted electrons to the conductor's atoms by collisions. The heat generated can be calculated by:

$$Q = I^2Rt = IVt \tag{1}$$

where Q is the amount of heat, I is the electric current flowing through a conductor, R is the electrical resistance of the material conductor, and t is the time.

Fig. 4 shows the measurements of electrical current and the induced temperature increase as a function of constant electrical voltage. The voltage was applied for 1 min at the electrodes, which were located 20 mm apart (Fig. 1) and sited over the surface of the coatings, that were doped with 8 (Fig. 4a), 10 (Fig. 4b), and 12 (Fig. 3c) wt% GNP. As expected, an increased applied voltage implies an increased electrical current and therefore a higher increase of the sample's temperature. However, it is worth noting that the I–V relationship is not linear, as was expected from Ohm's law. The electrical current exponentially increases with the applied voltage. This effect has been previously observed by other authors although it was not clearly explained [1].

I. Pelech et al. [18] recently published a study about the I–V characteristics of epoxy resins doped with carbon nanotubes. They found a nonlinear I–V ratio which could be well described by an exponential-type equation. The voltage increase induces an exponential grow of the electrical current, which could be the result of the positive temperature coefficient of conductivity of graphitic nanofillers; the increase in the power emitted on the electrical percolation paths causes their heating and leads to the increase of their conductivity. They confirmed that this I–V relationship can be defined by:

$$I = G\,V\,\exp(kV) \tag{2}$$

where I is the current (mA), V is the voltage (V), G is the electrical conductance at $V = 0$ V (S), and k is a constant, indicating the exponential ratio between current and voltage.

Fig. 4 shows the fitting of the experimental data with equation (2), and Table 1 collects the calculated parameters for fitting, specifically G and k. The electrical conductivity of each sample studied is then determined from the conductance and the geometry of the samples, based on equation (2).

It is worth noting that the thickness of the coating, necessary for the evaluation of the cross-sectional area, was measured for each sample using SEM. In order to verify the fitting equation, the electrical conductivity of the samples was also determined by Ohm's law in two different voltage ranges; conductivity at low voltages (0–200 V), and at high voltages (400–800 V). These results are also collected in Table 1 and in Fig. 4, together with the experimental data fitting by means of equation (2).

As was expected, the electrical conductivity of the samples increases with the GNP content. However, the electrical conductivity also increased with the applied voltage. This could be explained by the heating caused by Joule's effect, which is associated with the increase of the power emitted on the percolation paths [18]. The constant k, in equation (2), gives information about the dependence of the electrical conductivity on the voltage. The k value is highest for the coating with the lowest GNP percentage, meaning that the influence of voltage is higher for nano-doped samples with a nanofiller concentration close to the percolation threshold. With a higher GNP content, the increase in electrical conductivity at high voltages is less pronounced.

On the other hand, Fig. 4 also presents the temperature increase caused by Joule's effect. As shown by equation (1), the heat emitted

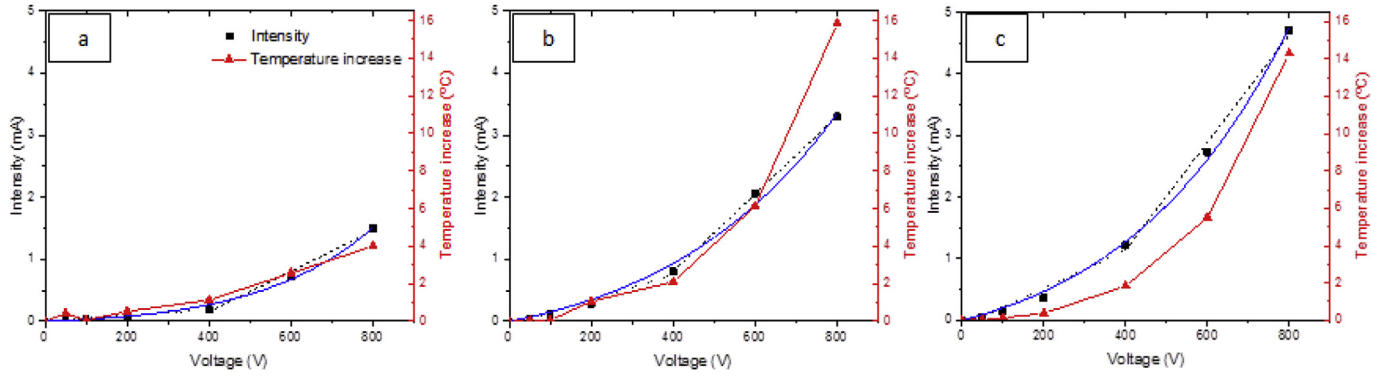

Fig. 4. Electrical current intensity (black square symbol) and increase of temperature (red triangle symbol) as a function of the electrical voltage applied for coatings doped with (a) 8, (b) 10, and (c) 12 wt% GNP. Experimental data fitting with equation (2) (blue solid line) and with Ohm's law at low and high voltage (black dotted lines). (For interpretation of the references to colour in this figure legend, the reader is referred to the Web version of this article.)

Table 1
Electrical parameters of GNP/epoxy coatings: electrical conductance G and the constant k, both determined with equation (2); and electrical conductivity at low and high voltages as calculated by Ohm's law.

wt% GNP	G ($\times 10^{-3}$) (mS)	k ($\times 10^{-3}$)	σ_0 ($\times 10^{-3}$) (S/m)	σ_{LV} ($\times 10^{-3}$) (S/m)	σ_{HV} ($\times 10^{-3}$) (S/m)
8	0.24	2.0	0.24	0.48	3.8
10	1.3	1.5	1.48	2.31	7.1
12	1.7	1.5	1.64	2.99	8.4

G is the electrical conductance when the voltage is zero.
k is a constant.
σ_0 is the electrical conductivity when the electric field strength is zero, determined from the conductance value calculated by equation (2).
σ_{LV} is the electrical conductivity calculated by Ohm's law at low voltages (0–400 V).
σ_{HV} is the electrical conductivity calculated by Ohm's law at high voltages (400–800 V).

directly depends on the applied voltage and the current intensity; both imply a greater temperature increase. For this reason, the heating is higher for the sample with highest electrical conductivity, corresponding to the epoxy coating doped with the highest GNP content, i.e. 12 wt% GNP.

The heating of the coating was homogenous in the whole area between the electrodes, caused by the high thermal conductivity of the epoxy resins doped with GNP [19–21].

Another important variable in this kind of system is time. Fig. 5a shows the increase of temperature as a function of time when a voltage of 800 V was applied. A fast temperature increase is measured in the first five minutes, then the temperature gradient in time is strongly reduced, indicating stability of the heat transfer process. The heating rate increases with the increase of GNP content of the nano-reinforced coatings, being 7.2, 10.3, and 13.6 °C/min for samples doped with 8, 10, and 12 wt% GNP respectively. Two different methods were used for temperature measurement; namely a thermocouple on the surface of the sample and an IR thermal camera (Fig. 5b). Both gave similar results, comparing the temperature measured in the middle of the sample.

The IR thermal camera also allowed analysis of the distribution of temperature over the samples' surface, thus determining the homogeneity of Joule's heating. In fact, the upper and lower edges of the samples between the electrodes show the highest temperatures. This means that the highest electrical current is in the edges; this phenomenon is known as the skin effect and is usually observed under alternating current (AC). Moreover, the thermal images, collected in Fig. 5b, show that the heating is not totally homogeneous, caused by the preferential electrical paths of the percolation network formed by the

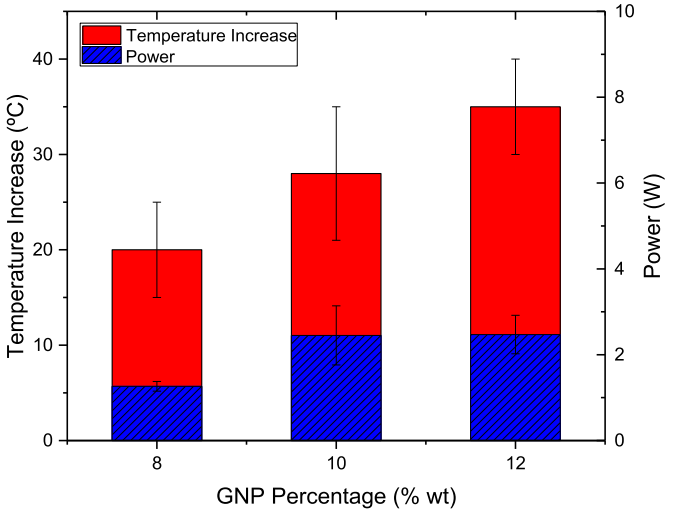

Fig. 6. Electrical power and the maximum increase of temperature reached by the application of 800 V at room temperature, as a function of the GNP percentage added to epoxy coatings.

GNPs. In fact, constant temperature paths perpendicular to the electrodes can be distinguished, thus evidencing the direction of the electrical current. It is however clear from Fig. 5b that increased GNP content allows for a more homogeneous flow of current and consequently, a more uniform temperature field between the electrodes.

Taking into account that the GNP/epoxy coatings are to be used in ADISs, the ice melting occurs when the temperature reaches 0 °C, starting from conventional atmospheric cold temperatures, i.e. from −10 to −40 °C, depending on the application scenario. Therefore, the increase of temperature needed in the studied materials should be in the range of 10–40 °C. These values are reached when the applied voltage is higher than 600 V for all studied coatings. The applied voltage is directly related to the power consumption:

$$P = I\,V \tag{3}$$

where P is the electrical power, I is the electrical current, and V is the applied voltage.

Fig. 6 shows the electrical power and the maximum temperature increase measured as a function of the GNP percentage with an applied voltage of 800 V. The application of this high voltage induces an important heating effect, with measured temperature increases of 20–40 °C. At the same voltage, the transported current increases with the GNP content due to the higher electrical conductivity and therefore

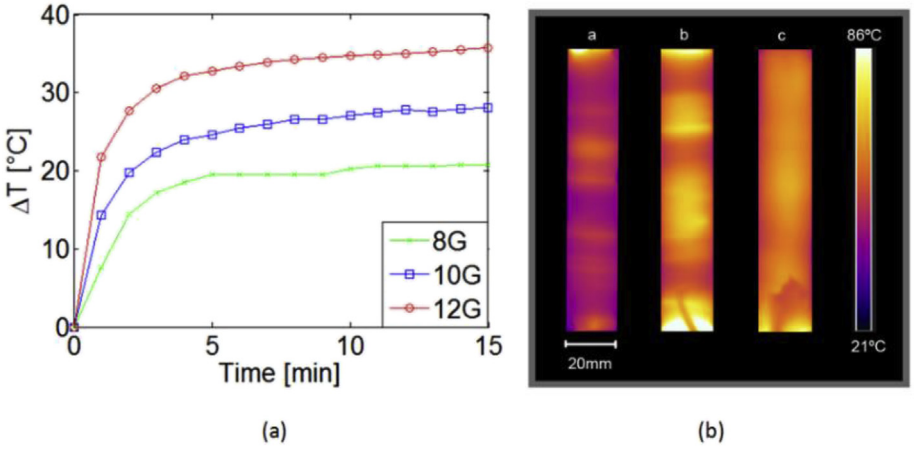

Fig. 5. Increase of temperature as a function of time applying 800 V. (a) Temperature measured by thermocouple over the surface and (b) thermal images captured by IR camera after 15 min for increasing GNP wt%, specifically a) 8 wt%, b) 10 wt%, and c) 12 wt%.

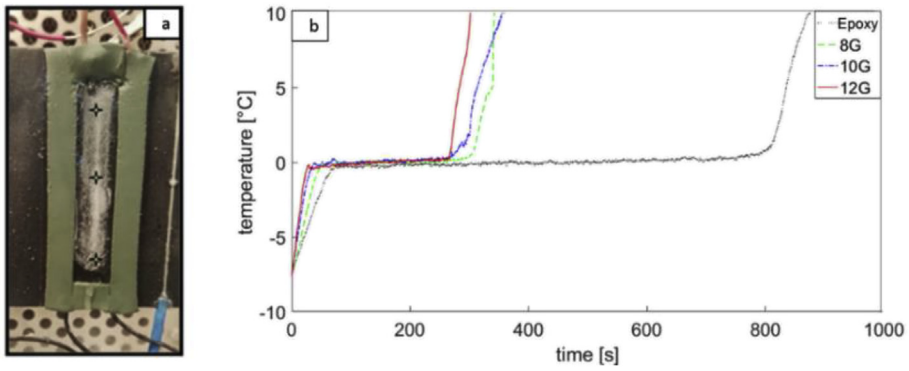

Fig. 7. De-icing tests at room temperature with an applied voltage of 750–800 V. (a) An image of the initial sample with ice over its surface and (b) variation of the surface temperature as a function of time for different GNP/epoxy coatings.

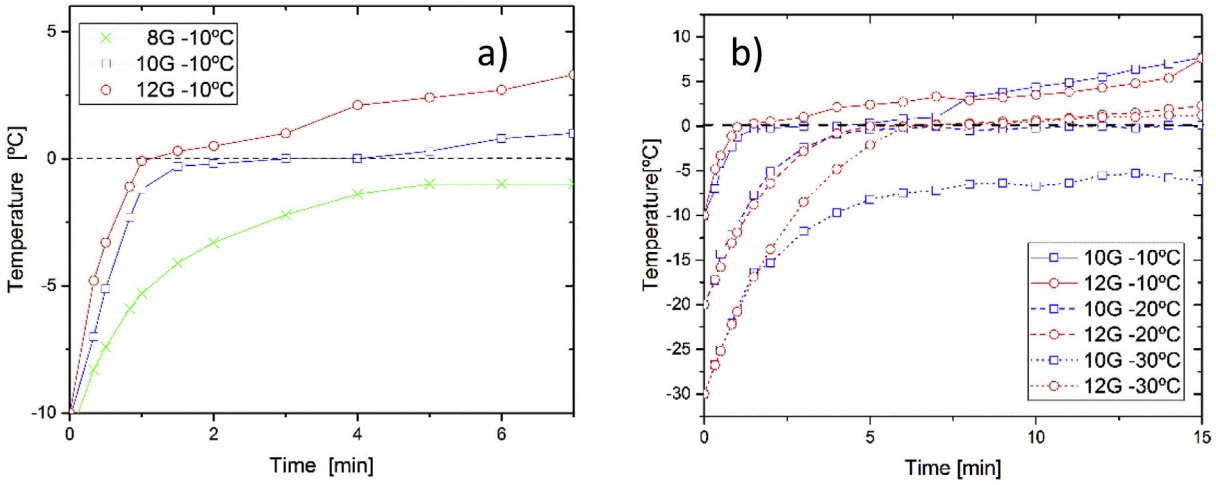

Fig. 8. De-icing tests at low temperature with an applied voltage of 750–800 V. Variation of surface temperature as a function of time: (a) curves at −10 °C for epoxy coatings doped with 8, 10, and 12 wt% GNP; and (b) curves at −10, −20 and −30 °C for epoxy coatings doped with 10 and 12 wt%.

both electrical power and temperature proportionally increase. In spite of the high value of applied voltage, the energy consumption is very low, in the range of 1–3 W. For comparison, the electrical power of a conventional light bulb is close 100 W and LED lights, which promote reduced power consumption, use around 25 W.

3.3. De-icing tests

Fig. 7 shows the de-icing tests at room temperature. The ice was generated at −15 °C over the sample surface, with controlled thickness, close to 3 mm. Then, the samples were hanged on a frame at room temperature and the de-icing process was accelerated by the application of a voltage in the range of 750–800 V, between the electrodes located 20 mm apart. A natural de-icing process was also executed at room temperature for a non-doped epoxy coating, which can be considered as a reference. The temperature was determined as the average value of three points over the sample surface (Fig. 7a), obtained with the thermal images captured with the IR thermal camera.

The de-icing curves (Fig. 7b) show three stages: 1) at the beginning, the sample temperature is below 0 °C because the ice was generated at −15 °C. Note that the curves do not start at −15 °C due to the temperature increase that occurred while passing the sample from the climatic chamber to the hanging configuration.

The temperature of the samples increases up to 0 °C, which is the melting point for water at atmospheric pressure; 2) the temperature remains constant at 0 °C, during solid–liquid transition; and 3) the temperature increases again after the solid–liquid transition is completed. Similar curves were previously obtained for epoxy/CNT samples [8]. The application voltage over the samples with GNP induces heating by Joule's effect and, as a consequence, the time for the solid–liquid transition is significantly decreased. This acceleration is slightly higher for the samples with higher electrical conductivity, which correspond to the coatings doped with higher GNP content. Without the ADIS, the ice takes 13 min to melt, whereas this time is reduced down to 5 min when the ADIS is activated.

One of the main advantages of the proposal ADIS in comparison with traditional de-icing devises is the quick response. The ice can be removed in a few minutes, however depending on the thickness and adherence of ice. For performance comparison, E. Enriquez et al. [1] published the heat transfer performance of carbon black coatings for anti-/deicing components, requiring up to 8–10 min to completely remove the ice at −18 °C, while the time necessary in our proposed ADIS, based on a CNT/epoxy coating, is close to 5 min at −15 °C. L. Chen et al. [22] have recently published results for the de-icing applications based on neat graphene coatings, processed by spraying. De-icing time decreases 42–72% with respect to the uncoated sample. In the present paper, a doped paint of easier application, reduces the time for ice melting by 62% with respect to the uncoated sample, specifically for the case with 12 wt % GNP content.

The study of the influence of temperature, at which the ice is formed, is interesting because the adhesion and quality of the ice can vary as a function of environment temperature. Fig. 8 shows the de-icing tests at low temperature (−10, −20, and −30 °C). The experiments are similar to the one at room temperature, but rather carried out in the climatic chamber at low temperatures. No reference sample was considered in this test. The same behaviour as for the room-temperature

test is obtained referring to the temperature–time curves, where three regions can still be identified in most of the samples. However, when the climatic chamber was set to −10 °C, for the coating with lowest nanofiller content, 8 wt% GNP (Fig. 8a), the temperature in the first step never reached 0 °C, thus preventing the activation of the solid–liquid transition.

In this case, the Joule's heating is not enough to remove the ice because the electrical current is too low (2.5 mA) at 750–800 V. For this system, higher voltages should be applied to obtain an effective ADIS coating. The 8 wt% GNP sample has thus been discarded for the subsequent analyses, when lower environmental temperatures have been considered, i.e. −20 and −30 °C (Fig. 8b).

At lower temperatures, the efficiency of the nano-reinforced coatings as ADIS are different. For example, at −10 °C, the ice melts at 5 and 1.5 min for coatings doped with 10 and 12 wt% GNP respectively, with similar applied voltages. At −30 °C, only the coating doped with 12 wt% was able to separate the ice from the substrate material. As the atmospheric temperature decreases, the time required to melt the ice is higher. The electrical current reached for each studied system justifies this behaviour, being higher for the coating with higher GNP content.

Table 2 collects the electrical resistance calculated from the applied voltage and the current measured for the de-icing test at different low temperatures. As was expected, the increase of GNP content on the coatings increases the electrical current flow, implying a more efficient ADIS coating. Interestingly, for the same sample at cryogenic temperatures, the electrical resistance slightly decreases when the temperature decreases. This behaviour is the opposite of that observed at room temperature, when the electrical conductivity increases with temperature. A similar behaviour is present in conventional conductor metals. Near room temperature, the electrical resistivity of most pure metals decreases monotonically with temperature, following an approximately linear relationship. This trend is the result of electron–phonon scattering, and it is the dominant temperature-dependent contribution to the resistivity. At low temperatures, the resistivity tends toward a constant value. However, these interesting results must be studied in depth in future works.

Fig. 9 shows different de-icing tests carried out to evaluate the repetitiveness and reliability of the reinforced samples and, in addition, the robustness of the de-icing tests designed. In fact, as no standard has been followed for the execution of de-icing tests, different repetitions of the same test have been executed in order to confirm the promising results described above.

First, the same de-icing test at low temperature is applied three consecutive times over the same sample (Fig. 9a) in order to evaluate 1) the repetitiveness of the test procedure and 2) if the efficacy of the ADIS coating varies with its use, though very preliminarily, as a higher number of repetitions are required for ageing characterisation. The obtained results confirmed that the efficiency remains constant. The time at which the ice melts is constant in the consecutive test repetitions. This was expected because the electrical conductivity of the doped coating remains constant; therefore the electrical current and the associated Joule's heating are stable.

Second, Fig. 9b shows the de-icing test applied to different specimens of the epoxy coating doped with 12 wt% GNP, manufactured with the same experimental conditions. No clear differences were observed, confirming the reproducibility of the applied manufacturing process. After applying a constant voltage at the electrodes, the time at which the ice melted, with a −10 °C environmental temperature, is equal for different samples with the same GNP content.

3.4. Anti-icing test

Fig. 10 shows images of the anti-icing test. The samples were introduced in a climatic chamber at −15 °C for 15 min with the ADIS activated. A constant voltage of 750–800 V was applied. In non-active regions, the thickness of the ice generated over the surface is in the range of 3–4 mm (Fig. 10d). However, ice formation is avoided on the active areas for the different coatings studied. The anti-icing efficiency is similar for all three samples studied, doped with 8, 10, and 12 wt% GNP.

It is worth noting that at −10 °C, the 8 wt% doped coating was not able to melt or separate the ice from the substrate in the de-icing test. However, at −15 °C, this system shows enough efficiency to avoid ice generation. This might suggest that the heat needed to remove the ice is higher than the heat required to avoid the ice generation. This can be explained by the fact that, for de-icing, an additional power corresponding to the enthalpy of fusion has to be provided for ice melting and, furthermore, for its separation from the substrate. On the contrary, for anti-icing, the liquid water mist directly increases its temperature while in contact with the coating, thus remaining liquid and avoiding ice formation.

The ADIS system studied in this work present numerous advantages regard conventional ADIS devices, such as quick response, low electrical power consumption, environmentally friendly and easy processing of coating.

4. Conclusions

GNP/epoxy coatings have been studied as an anti-icing and de-icing system ADIS, using their self-heating by Joule's effect. The thermoelectrical behaviour of epoxy coatings, with GNP contents above the electrical percolation threshold, has been analysed. They do not follow Ohm's law at room temperature; the electrical current increases exponentially with the applied voltage due to the self-heating of the sample's surface.

Different anti-icing and de-icing tests were designed to evaluate the behaviour, the efficiency, and the repeatability of the studied ADIS. With an applied voltage of 750–800 V, the epoxy coatings doped with GNP contents from 8 to 12 wt % GNP are suitable as anti-icing systems at −15 °C, aptly avoiding ice formation. However, higher GNP contents, 12 wt % GNP, are required if the system is to be used as a de-icing system, for melting the ice at very low temperatures up to −30 °C. This is due to the different heat transfer mechanisms involved in the de-icing and anti-icing processes. Although the applied voltage could be considered relative high, the power consumption is low, in the range of 1–3 W.

Finally, repeated tests have been made to confirm that the anti-icing and de-icing coating designed and verified in this study present promising performances and good reproducibility.

Table 2
Electrical parameters for de-icing tests at different low temperatures.

wt% GNP	−10 °C			−20 °C			−30 °C		
	V (V)	I (mA)	R ($\times 10^6$) (MΩ)	V (V)	I (mA)	R ($\times 10^6$) (MΩ)	V (V)	I (mA)	R ($\times 10^6$) (MΩ)
8	800	2.4	0.33	–	–	–	–	–	–
10	800	5.1	0.16	800	5.2	0.15	782	5.8	0.13
12	772	6.0	0.13	743	6.3	0.12	725	6.4	0.11

V is the applied voltage, I is the current, R is the electrical resistance, calculated with Ohm's law.

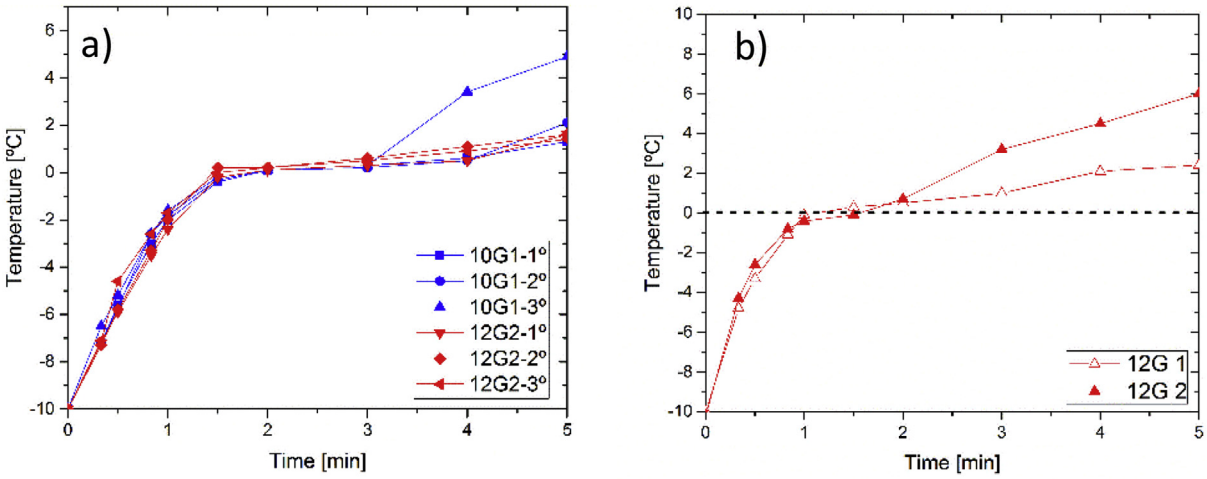

Fig. 9. Repeatability of the de-icing test procedure at (a) −10 °C with the same samples and (b) for different specimens with the same GNP wt%.

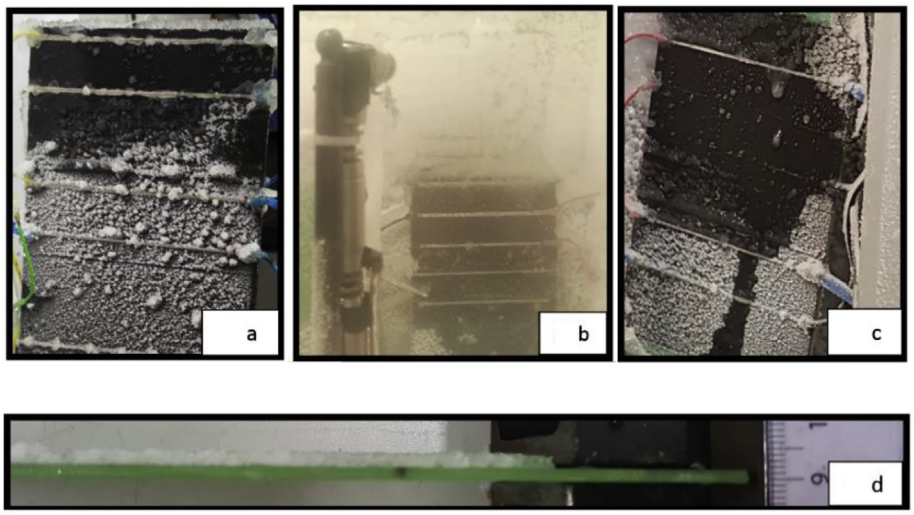

Fig. 10. Anti-icing test results at −15 °C with an applied voltage of 750 V on the epoxy coatings doped with (a) 8, (b) 10, and (c) 12 wt% GNP. (d) Cross-sectional picture of the epoxy specimen with ice formed on its surface.

Acknowledgements

The authors would like to express their gratitude to the Ministerio de Economía y Competitividad of the Spanish Government through the research project (MAT2016-78825-C2-1-R) and the PhD grants of O. Redondo (MAT2013-46695-C3-1-R, BES-2014-070371, and EEBB-I-2017-11991).

References

[1] E. Enríquez, J.F. Fernández, J. De Frutos, M.A. De la Rubia, Tailoring of the electrical properties of carbon black–silica coatings for de-icing applications, Ceram. Int. 41 (2) (2015) 2735–2743 Part B.

[2] S.K. Thomas, R.P. Cassoni, C.D. Mac Arthur, Aircraft anti-icing and de-icing techniques and modeling, 33 (5) (1996) 841–854.

[3] S. Farhadi, M. Farzaneh, S.A. Kulinich, Anti-icing performance of superhydrophobic surfaces, Appl. Surf. Sci. 257 (14) (2011) 6264–6269.

[4] R. Karmouch, G.G. Ross, Superhydrophobic wind turbine blade surfaces obtained by a simple deposition of silica nanoparticles embedded in epoxy, Appl. Surf. Sci. 257 (3) (2010) 665–669.

[5] Z. Zhang, et al., A novel thermo-mechanical anti-icing/de-icing system using bistable laminate composite structures with superhydrophobic surface, Compos. Struct. 180 (2017) 933–943.

[6] M. Campo, A. Jiménez-Suárez, A. Ureña, Effect of type, percentage and dispersion method of multi-walled carbon nanotubes on tribological properties of epoxy composites, Wear 324–325 (2015) 100–108.

[7] S.G. Prolongo, R. Moriche, M. Sánchez, A. Ureña, Self-stratifying and orientation of exfoliated few-layer graphene nanoplatelets in epoxy composites, Compos. Sci. Technol. 85 (2013) 136–141.

[8] H. Li, Q. Zhang, H. Xiao, Self-deicing road system with a CNFP high-efficiency thermal source and MWCNT/cement-based high-thermal conductive composites, Cold Reg. Sci. Technol. 86 (2013) 22–35.

[9] Q. Zhang, et al., Mechanically robust and electrically conductive graphene-paper/glass-fibers/epoxy composites for stimuli-responsive sensors and Joule heating deicers, Carbon N. Y. 124 (2017) 296–307.

[10] J. Li, P.S. Wong, J.K. Kim, Hybrid nanocomposites containing carbon nanotubes and graphite nanoplatelets, Mater. Sci. Eng. A 483–484 (1–2 C) (2008) 660–663.

[11] K. Chu, W.S. Li, H. Dong, Role of graphene waviness on the thermal conductivity of graphene composites, Appl. Phys. A Mater. Sci. Process. 111 (1) (2013) 221–225.

[12] A. Jiménez-Suárez, M. Campo, M. Sánchez, C. Romón, A. Ureña, Dispersion of carbon nanofibres in a low viscosity resin by calendering process to manufacture multiscale composites by VARIM, Compos. Part B Eng. 43 (8) (2012) 3104–3113.

[13] A. Jiménez-Suárez, M. Campo, I. Gaztelumendi, N. Markaide, M. Sánchez, A. Ureña, The influence of mechanical dispersion of MWCNT in epoxy matrix by calendering method: batch method versus time controlled, Compos. Part B Eng. 48 (2013) 88–94.

[14] R. Moriche, S.G. Prolongo, M. Sánchez, A. Jiménez-Suárez, M.J. Sayagués, A. Ureña, Morphological changes on graphene nanoplatelets induced during dispersion into an epoxy resin by different methods, Compos. Part B Eng. 72 (2015) 199–205.

[15] P. Xavier, Maldague, Theory and Practice of Infrared Technology for Nondestructive Testing, (2001) First.

[16] S.G. Prolongo, R. Moriche, A. Jiménez-Suárez, M. Sánchez, A. Ureña, Advantages and disadvantages of the addition of graphene nanoplatelets to epoxy resins, Eur. Polym. J. 61 (2014) 206–214.

[17] R. Moriche, M. Sánchez, A. Jiménez-Suárez, S.G. Prolongo, A. Ureña, Electrically conductive functionalized-GNP/epoxy based composites: from nanocomposite to

multiscale glass fibre composite material, Compos. Part B Eng. 98 (2016) 49–55.
[18] I. Pelech, K. Agnieszka, R. Pelech, Current-voltage characteristics of the composites based on epoxy resin and carbon nanotubes, J. Nanomat. 405345 (2015) 1–7.
[19] S. Chatterjee, F. Nafezarefi, N.H. Tai, L. Schlagenhauf, F.A. Nüesch, B.T.T. Chu, Size and synergy effects of nanofiller hybrids including graphene nanoplatelets and carbon nanotubes in mechanical properties of epoxy composites, Carbon N. Y. 50 (15) (2012) 5380–5386.
[20] F. Wang, L.T. Drzal, Y. Qin, Z. Huang, Enhancement of fracture toughness, mechanical and thermal properties of rubber/epoxy composites by incorporation of graphene nanoplatelets, Compos. Part A Appl. Sci. Manuf. 87 (2016) 10–22.
[21] S.G. Prolongo, R. Moriche, G. Del Rosario, A. Jiménez-Suárez, M.G. Prolongo, A. Ureña, Joule effect self-heating of epoxy composites reinforced with graphitic nanofillers, J. Polym. Res. 23 (9) (2016).
[22] L. Chen, Y. Zhang, W. Qiong, Effect of graphene coating on the heat transfer component, Coating 7 (158) (2017) 1–11.